Ceramics International 50 (2024) 43907–43917

Contents lists available at ScienceDirect

Ceramics International

journal homepage: www.elsevier.com/locate/ceramint

Compositional effects in potassium metakaolin geopolymers containing alumina and glass frit

Patrick F. Keane [a,*], Rhys Jacob [b], Martin Belusko [c], Waltraud M. Kriven [d], Nikki Stanford [a], Frank Bruno [a]

[a] Future Industries Institute, University of South Australia, Mawson Lakes, SA 5095, Australia
[b] Forschungszentrum Jülich GmbH, Institute of Energy Materials and Devices, Microstructure and Properties of Materials (IMD-1), Jülich, 52428, Germany
[c] Mondial Advisory Pty Ltd, Hyde Park, SA 5061, Australia
[d] Department of Material Science and Engineering, University of Illinois at Urbana-Champaign, Urbana, IL, USA

ARTICLE INFO

Handling Editor: Dr P. Vincenzini

Keywords:
Geopolymer
Porosity
Heat treatment
Alumina
Glass frit
Rheology
Viscosity

ABSTRACT

Geopolymers represent a distinct class of materials characterised by their X-ray amorphous nature and nanoporous, nanoparticulate structure. Geopolymers can be conveniently mixed, poured, and cured under ambient conditions. This makes this class of materials an interesting alternative to ordinary Portland cement for structural processes. Additionally, the addition of alumina can improve mechanical properties, while the addition of glass can form an impermeable glaze which could be useful for molten salt containment. Therefore, in this investigation, potassium metakaolin-based geopolymer composites with varying proportions of glass particles and alumina platelets were fabricated, cured, heat-treated, and analyzed to study the effects of composition on material properties. Various attributes including rheological properties, densities, mass loss, shrinkage, and porosities were compared. It was observed that certain compositions exhibited high viscosities, making high shear mixing challenging, while also displaying significant permeability that would hinder their ability to contain liquids without leakage. Additionally, certain samples showed reduced densities, suggesting potentially weaker mechanical properties; however, the investigation did not include a direct assessment of mechanical properties. The most promising candidates for containing liquids at high temperature contained 50 wt% KGP, 25 or 35 wt% glass powder, and 25 or 15 wt% alumina platelets, respectively. ASH-G slurries required a minimum of 65 vol% KGP to produce a homogenous material compatible with additive manufacturing. The minimum amount of glass phase to form surface glazes was 16 vol%. Only samples containing more glass phase than alumina phase produced glazed composites.

1. Introduction

Geopolymers (GP) are a covalently bonded, inorganic polymer consisting of mostly silicon, aluminium, and oxygen that form solid, X-ray amorphous, ceramic-like materials under ambient conditions [1,2]. Geopolymers are fire and acid resistant, thermochemically stable, able to immobilise toxic and radioactive materials, have higher compressive strengths compared to Ordinary Portland Cement (OPC), and can incorporate a variety of reinforcing or functional phases [3–10]. Synthesis of GPs traditionally requires an aluminosilicate precursor and alkali activator source, although formation of geopolymers under acidic conditions is possible [11]. Viable aluminosilicate precursors include a variety of industrial waste ash, volcanic rock and clay minerals, however, clay minerals, such as metakaolin, are generally more uniform and reproducible compared to volcanic rock or industrial ash [12–15]. Geopolymers can be cast at room temperature, into complex molds, and cured after as early as 24 h at 50 °C [16–18]. Geopolymers can also be further improved through the addition of particles or fibres [19–21]. By tailoring these additives, useful properties such as increased strength or toughness can be realised, improving their performance. For example, geopolymer composites containing alumina platelets have been shown to have excellent high temperature strength, yet can be made at room

Abbreviations: ASH-G, Amorphous Self-Healing Geopolymer; DSC, Differential Scanning Calorimetry; EDS, Energy Dispersive Spectroscopy; G1, Group 1; KGP, Potassium Geopolymer; KWG, Potassium Waterglass; MK, Metakaolin; SEM, Scanning Electron Microscope; TES, Thermal Energy Storage; XRD, X-ray Diffraction.

* Corresponding author.
E-mail address: patrick.keane@mymail.unisa.edu.au (P.F. Keane).

https://doi.org/10.1016/j.ceramint.2024.08.242
Received 19 June 2024; Received in revised form 1 August 2024; Accepted 14 August 2024
Available online 16 August 2024
0272-8842/© 2024 The Authors. Published by Elsevier Ltd. This is an open access article under the CC BY license (http://creativecommons.org/licenses/by/4.0/).

temperature [21]. Interestingly, using 12.7 mm chopped basalt fibres in a geopolymer composite not only increased flexural strength after heating to 1100 °C but also exhibited self-healing properties [22]. The addition of traditional bone ash also revealed to fill microcracks with glassy phase and future composites had intentional glass phase added [23].

By the basalt fibres and/or bone ash melting and partially filling cracks in the geopolymer microstructure the composite is self-healing. This observed phenomenon inspired the use of glass particulates with lower melting temperature and higher homogeneity. Studies have also been investigating additive manufacturing capabilities of geopolymer composites [24–27]. Other researchers have measured viscosity, yield stress, and thixotropic index to determine if a material is suitable for additive manufacturing. For this reason, the viscosities, and thixotropic indexes of systematically varied geopolymer slurries were measured in this study.

Due to similar fabrication capabilities and chemical compatibility, extensive comparisons have been made between geopolymers and OPC for applications in civil and structural engineering [28–31]. Besides civil and structural engineering, other applications of geopolymer composites include purification of heavy metals from water, CO_2 sequestration, refractory items, biomedical technologies, synthesis of functional ceramics, thermal energy storage, and molten salt containment, among others [20,32–38]. Given the need for increasing the capacity of thermal energy in the future, the containment of molten salt for thermal storage applications requires further development [39]. A suitable composite for molten salt containment must have high temperature mechanical strength, be thermochemically stable, and impermeable to fluids. Therefore, container materials for molten salts can be metal alloys, ceramics, or refractory composites. Common metal alloys such as stainless steel 304 and 316 have shown substantial levels of corrosion and require high purity inert atmospheres to contain molten salts [40–42]. Suitable alloys are not completely corrosion-proof, use rare metals, and are cost prohibitive [43,44]. Ceramics are more chemically inert than alloys but require a longer time and higher energy during formation by comparison [45]. Refractory bricks are affordable, chemically and thermally stable but require joins and mortars resulting in more material and higher cost while risking leakage. An alternative to these proposed solutions is geopolymer composites as they are relatively low cost, easier to manufacture, and require less energy and time to form [46–49].

Previous work has demonstrated the ability to manufacture an amorphous, self-healing geopolymer (ASH-G) which successfully contained molten sodium and potassium chloride at 800 °C for 240 h [36,50]. This investigation aims to optimise a three-component, potassium metakaolin-based geopolymer (KGP) containing alumina platelets and low melting glass frit powder to improve upon said design to contain molten salts at 800 °C. Material properties such as viscosity, shear thinning index, open and closed porosity, density, thermal mass and length change, and formation of surface glazing were measured. The parameters which are to be optimised include identifying the minimum glass to achieve glaze, minimum geopolymer slurry to maintain ease of manufacturing, and the alumina-to-glass ratio that results in a uniform surface glaze. Results were compared by the amount of KGP, alumina, and glass present to determine which formulations had potential to contain molten salt. Therefore, in producing such a material, a potentially lower cost, easier-to-manufacture, and longer-life option for molten salt containment could be realised.

2. Methodology

2.1. Geopolymer composite preparation

Potassium metakaolin-based, geopolymer (KGP) composites containing homogenously dispersed 50-μm alumina platelets and glass frit powder were synthesised identically to previous work [36,50]. The KGP chemical reactions can be seen below. First, a potassium alkali-activator source, commonly known as potassium water glass (KWG) or potassium metasilicate solution in Equation (1), was prepared over 24 h. Once all amorphous fumed silica of particle size 5–50 nm from Scott Chemical Pty Ltd., SiO_2, was dissolved into a solution of potassium hydroxide and water, a homogenous KWG was achieved and mixed with MetaMAX ® metakaolin. Potassium hydroxide was 85 % anhydrous and sourced from ChemSupply Australia. The resulting mixture, shown in Equation (2), began to react upon combination and therefore had to be high sheared at 2000 rpm using an IKA® RW 2000 mixer to maximise geopolymerisation and avoid unreacted phases.

$$2KOH + 2SiO_2 + 10H_2O \rightarrow K_2O \bullet 2SiO_2 \bullet 11H_2O \quad \text{(Eq. 1)}$$

Equation (1): Formation of potassium waterglass solution from SiO_2, deionised water, and KOH

$$[K_2O \bullet 2SiO_2 \bullet 11H_2O] + [Al_2O_3 \bullet 2SiO_2] \rightarrow [K_2O \bullet Al_2O_3 \bullet 4SiO_2 \bullet 11H_2O] \quad \text{(Eq. 2)}$$

Equation (2): Formation of potassium geopolymer from metakaolin clay and potassium waterglass solution.

Fifty-micrometer, alumina platelets from Micro Abrasives and 10–250 μm glass frit powder from Oceanside Glass and Tile were then high sheared into the de-aerated, wet geopolymer, respectively, and de-aerated again using a vibrating table. This wet, composite material can be called a wet ASH-G. The de-aerated wet ASH-G was then poured into cylindrical molds (H = 35 mm; ID = 38 mm) with one open end, and then cured in 100 % relative humidity at 23 °C for 7 days as shown in Fig. 1 below. After one week, ASH-G samples were removed from the curing chamber and PVC molds. Demolded samples were then placed in ambient laboratory conditions to bench dry and acclimate to lower relative humidity, similar to previous methods [50].

Eight potential ASH-G compositions were selected by varying KGP, alumina platelets, and glass frit amounts. Geometrically measured and reference bulk densities of individual phases can be seen in Table 1 below. Compositional selections can be seen in Table 2, Figs. 2 and 3. At least three specimens for each sample composition were used to approximate material properties and corresponding error.

2.2. Workability measurement

De-aerated geopolymer composite slurries from Table 2 were mixed to homogeneity according to the method mentioned earlier. Samples were then taken and placed in a Netzsch Kinexus Pro+® rheometer using a parallel plate configuration as shown in Fig. 4. An upper plate with a diameter 20 mm was used as the ASH-G slurry has a relatively

Fig. 1. Wet ASH-G in cylindrical molds before curing for 7 days. Only the largest cylinders were used.

Table 1
Densities of alumina-glass-geopolymer phases.

Phase	Reference bulk density (g/cm^3)	Measured bulk density (g/cm^3)
KGP	1.47 [51]	1.86 ± 0.1
Glass Frit	2.5 [52]	2.47 ± 0.1
Alumina Platelets	3.97 [53]	3.88 ± 0.1

Table 2
Compositions of ASH-G samples.

Weight percent			Sample Set	Volume percent		
KGP	Al_2O_3	Fusing Glass		KGP	Al_2O_3	Fusing Glass
50	35	15	1	70	18	12
40	40	20	2	60	22	18
40	20	40	3	56	10	33
45	35	20	4	65	18	17
55	30	15	5	73	15	12
55	25	20	6	72	12	15
50	25	25	7	68	12	20
50	15	35	8	66	7	27

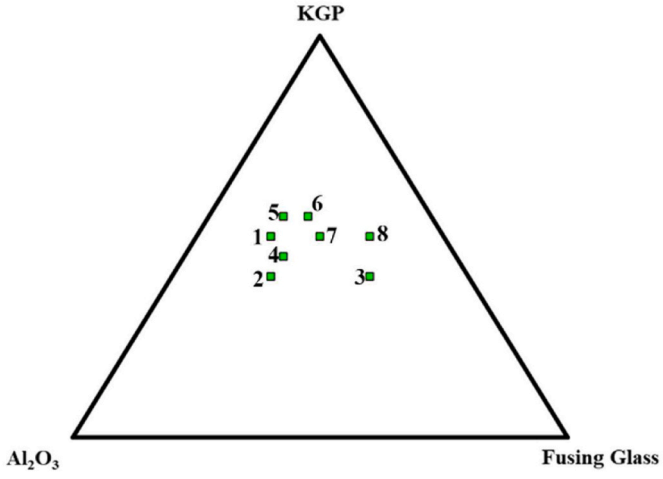

Fig. 2. Compositional ternary diagram of ASH-G composites (weight %).

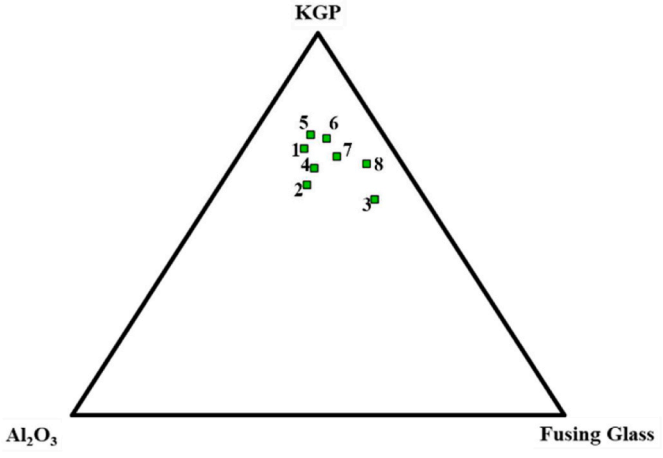

Fig. 3. Compositional ternary diagram of ASH-G composites (volume %).

Fig. 4. Kinexus Pro + rheometer used to measure yield stress and viscosity. The bottom and top plates are not included in this photo.

high viscosity [54]. Additionally, a measuring gap of 2.5 mm was selected which is 10 times larger than the largest particle, in this case the glass frit of 250 μm. This was done to remove any particle-particle jamming or interfering effects [55,56].

Homogenous ASH-G wet slurries of KGP, alumina platelets and glass frit from Table 2 were placed on the bottom plate of the Kinexus rheometer and top plate lowered into position. Next, any extra slurry was carefully removed using a spatula. Once the correct amount of sample (~5 g) was loaded, the shearing profile began [57]. Slurries were subjected to a shear rate of 1.0 sec^{-1} for 120 s followed by 10 sec^{-1} for 60 s and finally 1.0 sec^{-1} for 120 s. Fig. 5 below shows the previously described shear profile as a function of time. The profiles were selected to mimic an additive manufacturing extrusion process. Data points were taken every 0.1 s. Average viscosities were measured for low and high shear sections. Shear thinning indices of ASH-G samples were calculated using Equation (3) below [57–59]. All tests were done under ambient conditions. A temperature controlled lower plate was kept at 22 °C to minimise temperature effects.

$$Shear\ Thinning\ Index = \frac{\eta_{Low\ Shear}}{\eta_{High\ Shear}} \qquad \text{Equation 3}$$

Equation 3. Shear thinning indices comparing average viscosity at low and high shear rates.

2.3. Heating/sintering

Cured composites were demolded and acclimated to ambient humidity for 48 h before being placed into an electric muffle furnace using an air atmosphere. Composites were then heated to 900 °C for 5 h using heating and cooling rates of 1 °C/min, respectively. Heat-treated samples were removed from the furnace and labelled.

2.4. Mass/length change, density and open porosity

Geopolymer composite weights, heights and diameters were measured using a mass balance accurate to 0.01g and calipers accurate to 0.01 mm. Measurements were taken before and after heat treatment. Heat-treated, sample densities and open porosities were measured using the Archimedes method outlined in ASTM C20. Deionised water at 24 °C was used as the reference fluid. Samples were dried at 120 °C for 24 h

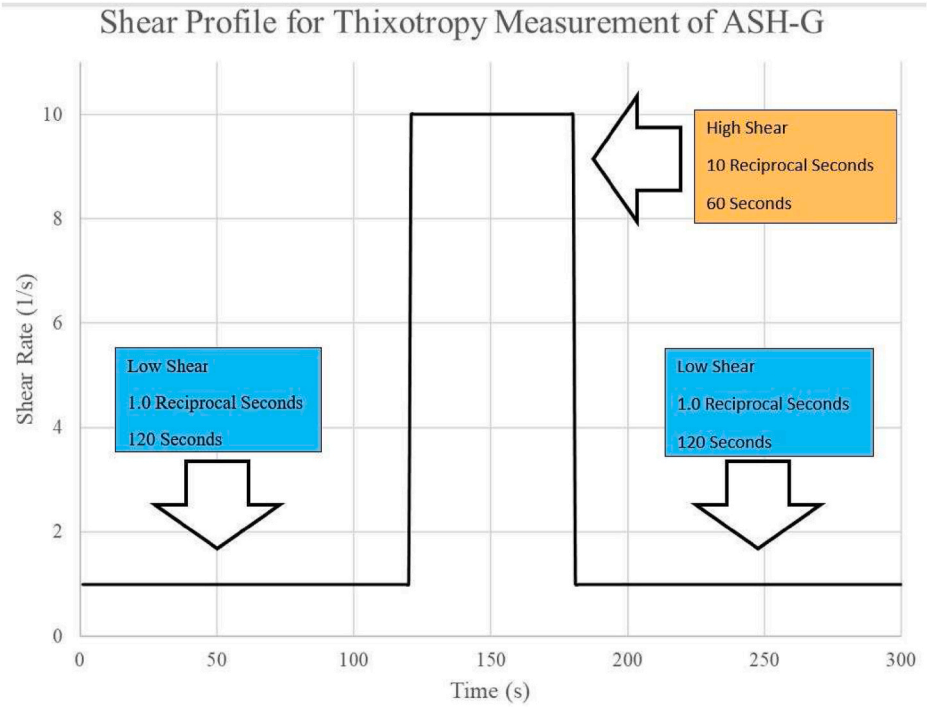

Fig. 5. Shear profile for determining rheological properties of ASH-G slurries.

and weighed, denoted by W_{Dry}. Next, samples were submerged in boiling water for at least 2 h to fill all open pores with fluid. Once cooled for at least 12 h and still submerged, suspended samples were weighed to offset buoyant force, W_{Sub}. Finally, surfaces of saturated samples were wiped of free water and weighed, W_{Sat}. Equation (4) through Equation (8) below show how to calculate open porosity and bulk density using described sample weights.

$$\mathbf{V_{Bulk}} = \frac{(\mathbf{W_{Sat}} - \mathbf{W_{Sub}})}{\rho_{Water}} \quad \text{Equation 4}$$

Equation (4). Bulk Volume

$$\mathbf{V_{Open\ Pores}} = \frac{(\mathbf{W_{Sat}} - \mathbf{W_{Dry}})}{\rho_{Water}} \quad \text{Equation 5}$$

Equation (5). Open Pore Volume

$$\mathbf{V_{Matrix}} = \frac{(\mathbf{W_{Dry}} - \mathbf{W_{Sub}})}{\rho_{Water}} \quad \text{Equation 6}$$

Equation (6). Apparent Volume

$$\rho_{\mathbf{Bulk}} = \frac{\mathbf{W_{Dry}}}{\mathbf{V_{Bulk}}} = \frac{\mathbf{W_{Dry}} * \rho_{Water}}{(\mathbf{W_{Sat}} - \mathbf{W_{Sub}})} \quad \text{Equation 7}$$

Equation (7). Bulk Density

$$\mathbf{Open\ Porosity} = \frac{\mathbf{V_{Open\ Pores}}}{\mathbf{V_{Bulk}}} = \frac{\mathbf{W_{Sat}} - \mathbf{W_{Dry}}}{\mathbf{W_{Sat}} - \mathbf{W_{Sub}}} \quad \text{Equation 8}$$

Equation (8). Open Porosity.

Beside the Archimedes method of determining density, the rule of mixtures and geometric methods were also used. The calculated method involved the summation of individual volume percents multiplied by corresponding density as seen in Equation (9). Geometric densities were calculated by dividing the mass of a sample by the volume of the sample, Equation (10). Finally, densities calculated by the Archimedes method relied on displaced reference fluid and difference of buoyant force and sample mass as described previously in Equation (7).

$$\rho_{Composite} = \sum_{i=1}^{n} [Volume\ Fraction_{\ i} * \rho_i] \quad \text{Equation 9}$$

Equation (9). Calculated Density via Rule of Mixtures

$$\rho_{Composite} = Mass_{Sample} / Volume_{Sample} \quad \text{Equation 10}$$

Equation (10). Geometric Density.

2.5. Microcharacterisation

Heat-treated samples were wet cut using a Brillant 240 saw and polished on a Struers Tegra grinding system using silicon carbide paper of 180, then 1200 grit, respectively. Further polishing was done on a Presi Mecatech 250 polishing system down to 6 μm, using diamond paste. A benchtop Hitachi TM4000 SEM was used to collect micrographs of uncoated polished cross sections. Surface glaze as well as internal, closed porosity percentages were averaged using ImageJ software. ImageJ software successfully identified closed pores based on grey scale micrographs. At least four, 6.25 mm^2, non-consecutive micrographs were used to determine closed porosity. Surface glaze thicknesses were based on at least two non-consecutive sections, each approximately 1 mm in length and from random heights along the cylinder.

3. Results and discussion

Geopolymer composites containing 50-μm alumina platelets and glass particulates, as seen in Fig. 6, were manufactured, cured for seven days, and heated to 900 °C for 5 h. The high angularity of these particles allowed for a relatively high average free space among particles [60]. It is hypothesized that this high average free space among particles allowed for molten glassy phase to flow throughout the composite more easily.

The packing density of alumina platelets and glass frit particles were assumed to be relatively homogenous and no phase separation present in room temperature samples was found.

ASH-G samples were cylindrical in shape and can be seen in Fig. 7

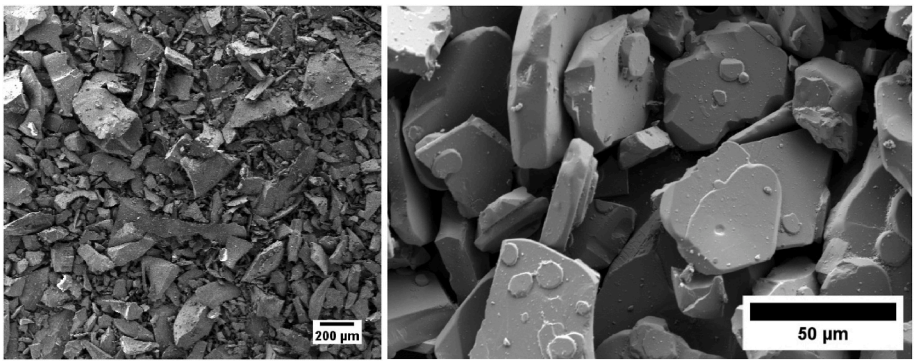

Fig. 6. Glass particles as received (left), alumina platelets as-received (right).

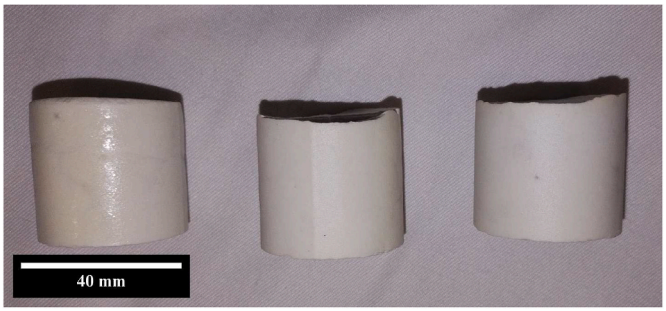

Fig. 7. Side view of cylindrical ASH-G samples after sintering at 900 °C for 5 h.

below. Average cylindrical diameters and heights were approximately 38 mm and 35 mm, respectively. Initial sample weights and dimensions were recorded after demolding and acclimating to ambient humidity. Weights and dimensions of samples after heating to 900 °C for 5 h were also recorded. The mass loss and shrinkage of multiple samples can be seen in Fig. 12 in a later section.

3.1. Rheological properties

As mentioned, shear stress and corresponding viscosities were collected every 0.1 s. The profile was selected to emulate an additive manufacturing extrusion process [61]. When a material is at rest or waiting to be pumped through a nozzle, little to no shearing occurs. Once a material is pumped and extruded, high shear rates are present. After deposition, the feed material is again in a low shear rate state. It has been demonstrated that metakaolin based geopolymer composites are thixotropic and experience reversible shear thinning [25,26,62].

It has been hypothesized and confirmed that the viscosities of ASH-G samples were inversely proportional to the amount of liquid phase present, i.e., composites with more KGP were less viscous (Fig. 10). The degree of shear thinning was determined by comparing average viscosities of final, low shear segments with high shear segments. Example data can be seen in Figs. 8 and 9. Pure KGP without additives had a much lower average viscosity than ASH-G samples which contained additives. All samples exhibited time-dependent viscosities when beginning a segment. For high shear segments, viscosities gradually decreased and for final, low shear segments, viscosities gradually increased. This gradual, time-dependent increase is called thixotropic behaviour.

The trend for initial, low-shear segments to have such high viscosities can be attributed to several factors. Intermolecular forces such as electrostatic potentials, dipole-dipole interactions, and even hydrogen bonding have been known to affect metakaolin-based geopolymer rheology [63]. The loss of water due to surface wetting of solid additives also increases viscosity [64]. When high sheared, agglomerates and partially formed long range networks in the geopolymer phase are disrupted, reducing the viscosity [63]. More significantly, the orientation of high aspect ratio platelets and particulates are random before high

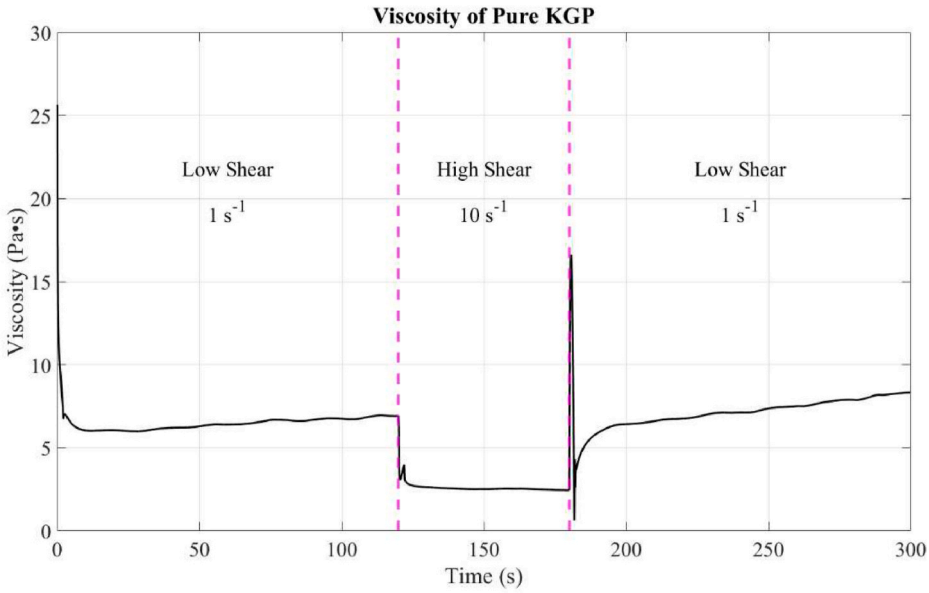

Fig. 8. Viscosity of pure KGP 10 min after initial mixing.

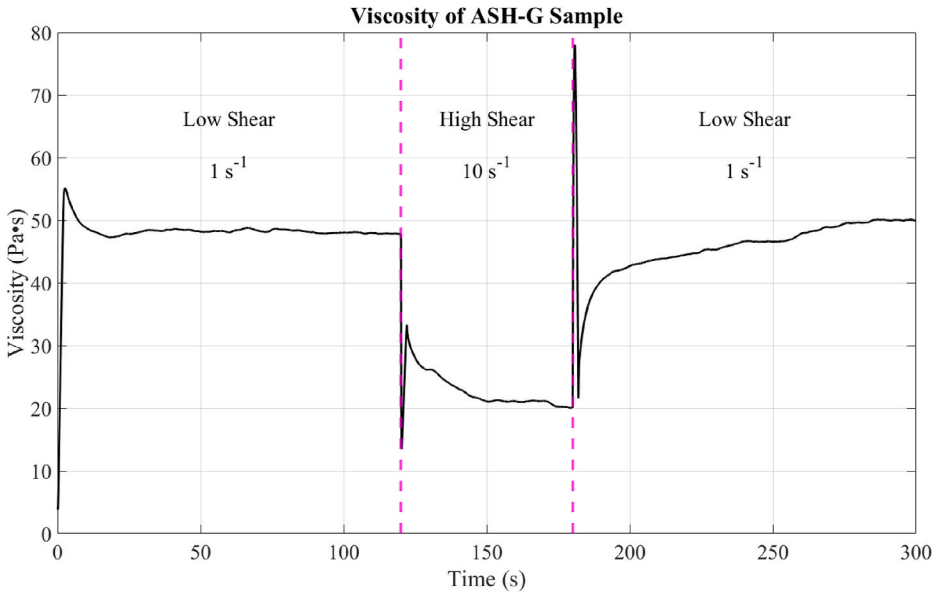

Fig. 9. Example viscosity results of ASH-G #6, 10 min after initial mixing.

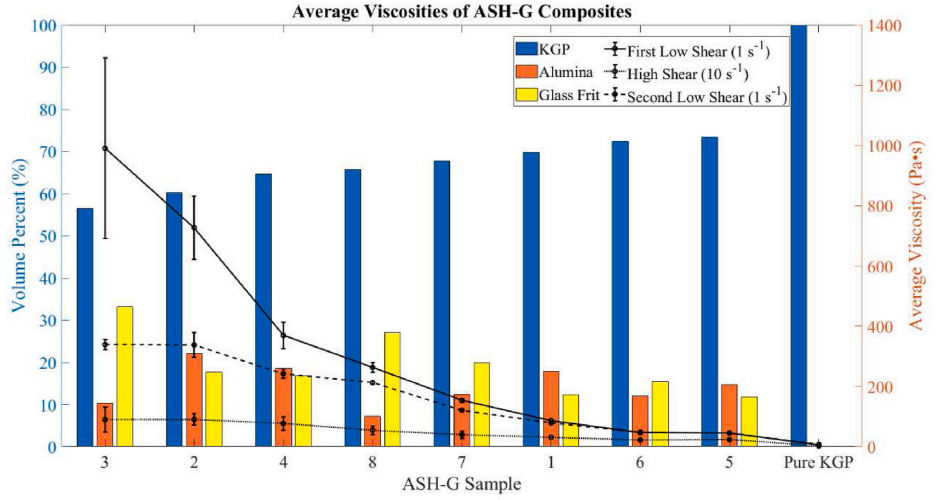

Fig. 10. Averaged viscosities of ASH-G composites. Shearing indices were determined from high shear and 2nd low shear data.

shearing, trapping water in voids and increasing viscosity. After high shearing, platelets are more likely to orient parallel to the direction of flow and flatten, allowing more water to become available, ultimately reducing viscosity. After this change in platelet and particulate orientation, the apparent viscosity at low shear rates is less than the original viscosity in which platelets were randomly oriented, causing a thixotropic effect as seen in Fig. 9.

Fig. 10 below compares the average viscosity of composites after mixing for 10 min, similar to sample preparation in the methodology section. Initial low shear segments possessed the highest viscosities, followed by final low shear segments and lastly, high shear segments in all cases. These results indicated that all wet ASH-G slurries were non-Newtonian fluids, including pure KGP. Additionally, because viscosities were lower at higher shear rates compared to lower shear rates, the slurries were a shear thinning fluid.

As mentioned, the shear thinning index was calculated by comparing the average visocities of the second low shear segments with high shear segments. Tabulated viscosites and shear thinning indices are displayed in Table 3 below. While the shear thinning index was an important value to estimate pumpability and flow properties, the viscosities were equally important. ASH-G samples 2, 3 and 4, due to their high solid loading content, were diffcult to mix initially using a high shear impeller and often exhibited a solid-like behaviour, as illustrated in Fig. 11. Samples with a minimum KGP content of 65 vol % could be mixed with a high shear impeller without the chopping phenomena in Fig. 11. Therefore, it

Table 3
Viscosities and shear thinning indices of ASH-G samples.

2nd Low Shear Viscosity (Pa•s)	High Shear Viscosity (Pa•s)	Shear Thinning Index	ASH-G Sample	KGP (vol%)
339.0	90.2	3.76	3	56.4
337.9	90.9	3.72	2	60.2
242.3	77.2	3.14	4	64.6
212.7	55.0	3.87	8	65.7
121.2	40.6	2.98	7	67.7
79.2	31.6	2.51	1	69.8
46.6	22.2	2.10	6	72.4
44.9	23.3	1.93	5	73.5
7.3	2.5	2.87	Pure KGP	100

Fig. 11. ASH-G samples 2, 3 and 4 behaved more as a solid than a liquid (left). Instead of flowing, samples would tear upon mixing with a high shear impeller (right).

can be concluded that samples containing at least 65 vol% KGP could have additive manufacturing capabilities.

3.2. Mass and length change after sintering

Of the three phases found in an ASH-G, only KGP experienced mass loss upon heating to 900 °C. This was due to the high amount of water found in KGP which was released primarily below 250 °C [65]. Potassium metakaolin-based geopolymer also experienced an appreciable amount of linear shrinkage when heating to 900 °C with the onset of shrinkage occurring at 140 °C due to water removal. This was followed by another regime of shrinkage due to crystallization into leucite beginning at 875 °C [66].

Alumina platelets are inert to this temperature and previous XRD results showed no interactions among the three phases [50]. Glass frit powder, while not chemically reacting or changing mass after heating, did experience melting and ultimately a small amount of length change. Therefore, most length changes and nearly all mass changes shown in Fig. 12 can be attributed to the KGP phase. Minimal linear length change is important because it reduces the amount of uneven three dimensional shrinkage which occurs during sintering, causing cracks and failure of the structure [21].

3.3. Densities and open porosity

Density measurements were averaged, and reported errors where available are seen in Fig. 13. Values ranged from 2.17 to 2.56 g/cc, which is a difference of approximately 16.5 %. Alumina platelets were the phase which was found to have the most direct effect on sample density. Even though alumina did not undergo length or mass change after heating to 900 °C, alumina was already a relatively dense material, ~4.00 g/cc [53], increasing the density of the composite. Secondly, KGP underwent densification upon sintering at ~900 °C [50]. Glass frit powder did not have a grain density increase after heating to 900 °C but any voids were filled by molten glass, increasing the bulk density. Sintering of KGP and the presence of liquid molten glass particles operated simultaneously and the effect was analogous to liquid phase sintering.

The Archimedes method mentioned in the previous section was also used to measure accessible, or open, porosity of ASH-G samples shown in Fig. 14. The amount of liquid a material can contain is closely related to how permeable the material is. Each phase in an ASH-G sample affected open porosity. Alumina platelets had a very low porosity but did not pack densely, resulting in many angular open channels which can be seen in Fig. 15 below [21]. Glass frit powder also had low open porosity, but a higher packing fraction preventing the possibilities of air entrapment during mixing [60]. Potassium GP had the highest open porosity of the three phases in an ASH-G, yet had the highest packing fraction, as it was the only liquid phase during formation. The highest amount of open porosity after heat treating ASH-G samples occurred in samples with the least amount of glass frit powder. The migration of molten glass in an ASH-G during heat treating also resulted in the formation of a surface glaze as shown in the next section, and greatly affected open porosity.

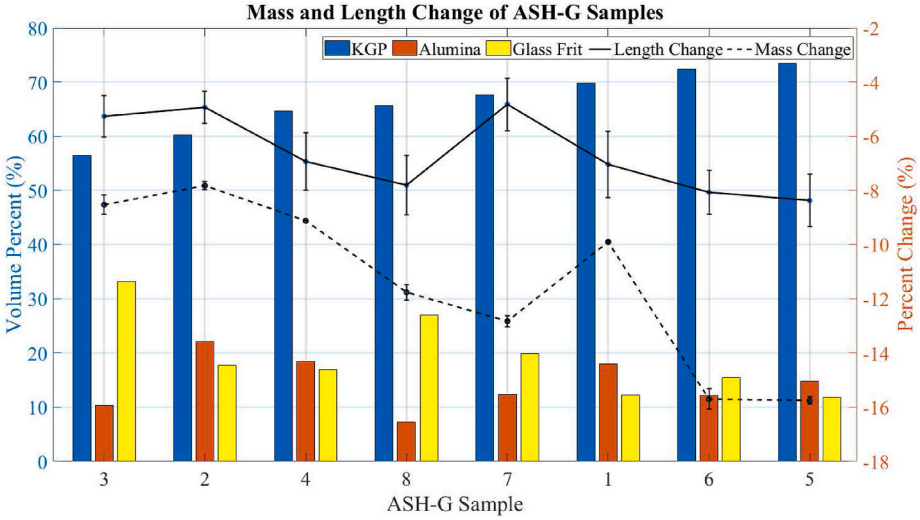

Fig. 12. Mass and length changes of ASH-G samples heated to 900 °C in order of increasing KGP content.

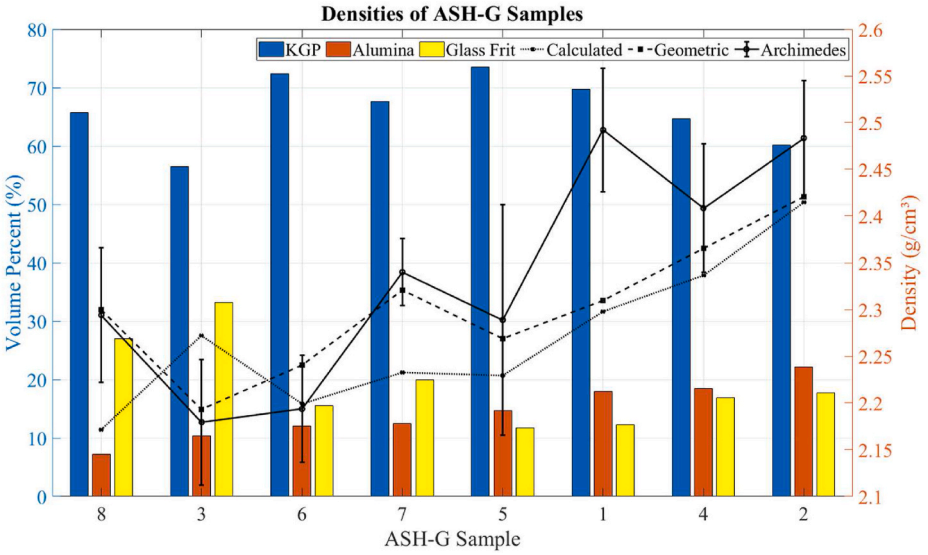

Fig. 13. Densities of ASH-G samples using rule of mixtures, geometric, and Archimedean methods in order of increasing alumina content. Pure KGP had a density of 2.0481 g/cm^3.

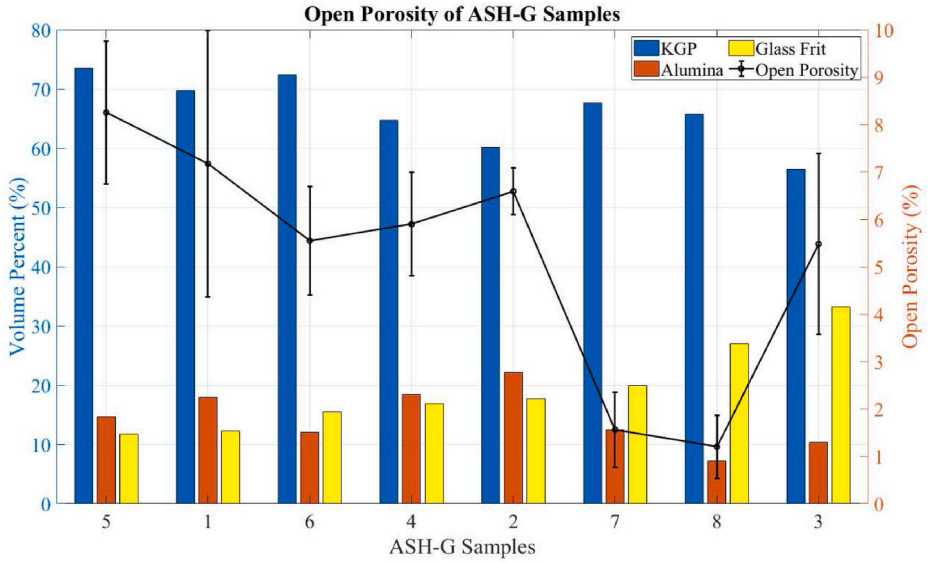

Fig. 14. Open porosity of ASH-G samples measured using the Archimedes method in order of increasing glass content.

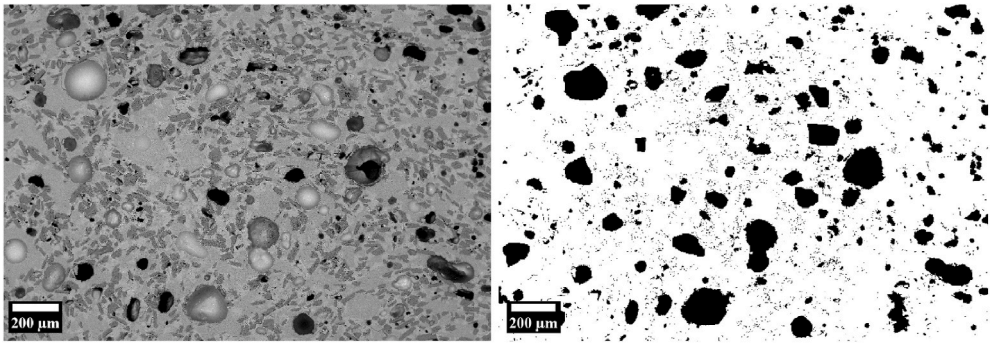

Fig. 15. Example SEM micrograph of ASH-G sample 4 (left) used by ImageJ (right) to determine closed porosity.

The relatively high open porosity in Sample 3, which contained little alumina platelets, could be attributed to destabilised shape change during sintering and internal cracking/swelling.

3.4. Closed porosity and glaze thickness

Closed, or inaccessible, porosity was measured using polished cross sections, microscopy, and image analysis software. Analysis using ImageJ separated out pores as areas based on relative contrast. Fig. 15 below is an example of how closed porosity was identified. ImageJ software was also used to measure glaze thickness of a given section, again based on grey scale contrast.

Closed porosity in ASH-G samples was attributed to several factors. The most significant was entrapped air during curing. The previous rheological results indicated that samples 2,3 and 4 behaved like a solid during the mixing phase. The amount of entrapped air was directly related to the viscosity of wet ASH-G slurries. Air bubbles were more likely to be trapped in a tortuous path found in ASH-G samples containing high amounts of additives. Additionally, high aspect ratio additives such as alumina platelets were more of an obstacle to air bubbles than lower aspect ratio additives [67].

Closed porosity results are shown in Fig. 16 below. During sintering, alumina platelets had little to no mobility, which did not directly affect ASH-G closed porosity [21]. The dehydration and restructuring of KGP at 900 °C led to a more dense amorphous geopolymer. The incorporation of alumina platelets, however, partially prevented this densification [21]. The glass particulates began to soften at ~600 °C and by 900 °C were less viscous [50,68]. Concurrently, capillary pressures and localised stresses on molten glassy phase during KGP sintering caused voids to be filled. The average distance between inert alumina platelets and glass particulates is critical to the ASH-G self-healing mechanism. In some cases, glass phase migrated to free surfaces, resulting in a homogenous impermeable glaze which greatly affected open porosity and apparent density, as shown in Figs. 17 and 18.

Table 4 below summarizes rheological and material properties as well as sintering behaviour of ASH-G composites by components. The mass loss and linear shrinkage after sintering was primarily due to the KGP phase with a minor effect from the glass frit softening during sintering. As expected, density was primarily attributed to densified alumina content. In nearly all cases, both open and closed porosity and glaze thickness were determined by the amount of glass frit content. Furthermore, the need for correct weight ratio of KGP:alumina:glass was easily seen when comparing open and closed porosities. A 50:15:35 composite was able to produce a surface glaze and have little to no open porosity. Alternatively, a 40:20:40 composite, which had relatively more glass and should be less porous had a higher open porosity. This is most likely due to rapid gas release and/or uneven heating during sintering. The viscosity and shear thinning index are directly attributed to KGP content as it is the only liquid phase.

4. Conclusions

The suitability of potassium metakaolin-based geopolymers containing alumina platelets and glass particulates to contain molten salts was previously investigated [36]. Material properties of composites before and after sintering included slurry viscosity, shear thinning index, mass and length changes, open and closed porosity, density, and presence of surface glaze were determined. The metastable balance among KGP, alumina platelets, and low melting glass particulates to form ASH-G bodies has a compositional tolerance as outlined below.

Samples with KGP:alumina:glass ratios of 50:25:25 and 50:15:35 are both recommended to be container material of molten salt. The ease of manufacturing, low starting materials cost and sintering temperature indicate these formulations are a readily available solution to containing molten salt. Samples containing 25 wt% alumina and 25 wt% glass frit had a higher amount of alumina implying more crack deflection, as well as enough self-healing phase to produce an impermeable glaze after sintering.

From the study it could be concluded that.

1. Wet ASH-G slurries require a minimum of 65 vol% KGP to produce a homogenous material by high shear mixing.
2. Homogenous ASH-G slurries have a large enough shear thinning index to potentially be used in additive manufacturing.
3. The amount of alumina platelets significantly affected linear shrinkage (5–8%) and density (2.16–2.56 g/cm^3). Samples with higher amounts of alumina platelets underwent less linear shrinkage and averaged higher densities before and after heating to 900 °C.
4. The minimal amount of glass phase to form surface glazes was 16 vol %.
5. Only samples containing more glass phase than alumina phase produced glazed composites.

Future work includes evaluation of mechanical properties at a variety of temperatures, feasibility of additively manufactured ASH-G

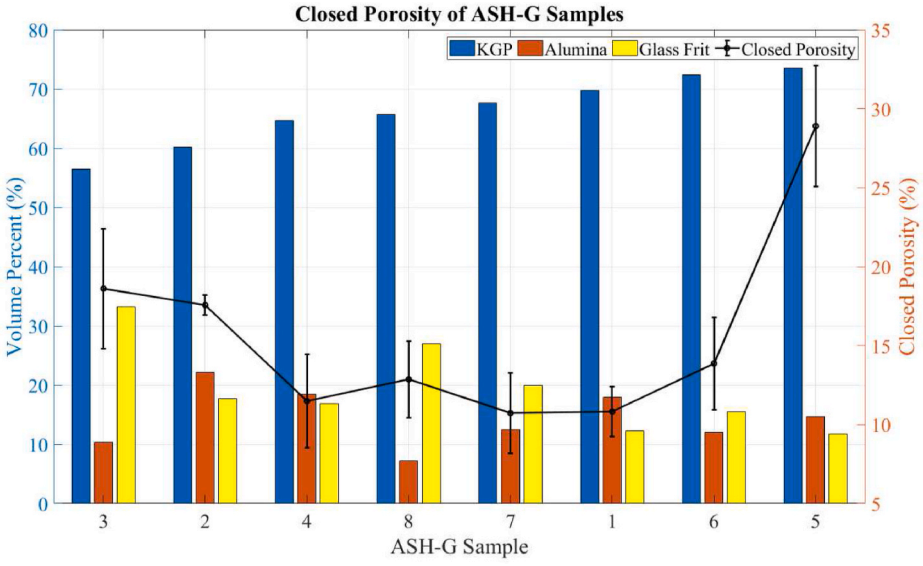

Fig. 16. Closed porosity of ASH-G samples using imaging software in order of increasing glass content.

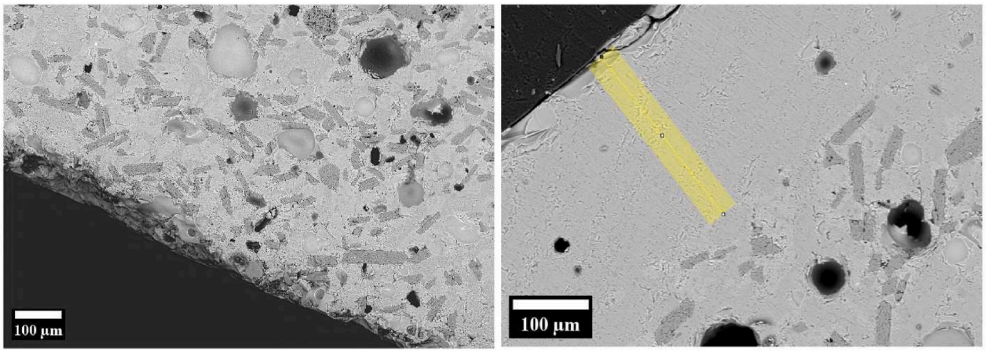

Fig. 17. Micrographs of ASH-G sample without (left; ASH-G 4) and with (right; ASH-G 6) a uniform glaze.

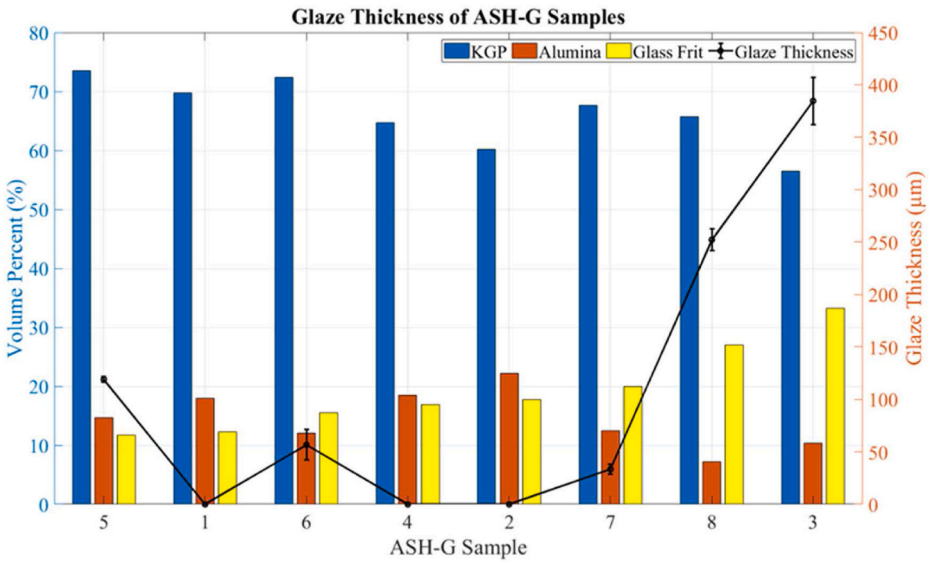

Fig. 18. Surface glaze of ASH-G samples using imaging software in order of increasing glass content.

Table 4
Summary of components on material properties.

Property	KGP	Alumina Platelets	Glass Frit
Mass loss after heating	↑	↓	↓
Linear shrinkage after heating	↑	↓	↑
Density	↓	↑	–
Open porosity	↑	–	↓
Closed porosity	↑	–	↓
Surface glaze	↓	↓	↑
Viscosity	↓	↑	↑

composites to contain molten salt, estimates of tortuosity from rheological data, and other possible additives such as silicon carbide for rapid microwave heating.

CRediT authorship contribution statement

Patrick F. Keane: Writing – review & editing, Writing – original draft, Visualization, Validation, Software, Methodology, Investigation, Formal analysis, Data curation, Conceptualization. **Rhys Jacob:** Writing – review & editing, Visualization, Validation, Supervision, Resources, Project administration, Investigation, Funding acquisition, Formal analysis, Data curation, Conceptualization. **Martin Belusko:** Writing – review & editing, Supervision, Resources, Project administration, Funding acquisition. **Waltraud M. Kriven:** Writing – review & editing, Supervision, Resources, Project administration, Funding acquisition. **Nikki Stanford:** Writing – review & editing, Supervision, Resources, Funding acquisition. **Frank Bruno:** Writing – review & editing, Validation, Supervision, Project administration, Funding acquisition.

Declaration of competing interest

The authors declare that they have no known competing financial interests or personal relationships that could have appeared to influence the work reported in this paper.

Acknowledgements

The authors acknowledge Microscopy Australia for use of facilities at the Future Industries Institute at the University of South Australia at Mawson Lakes. The authors thank Scott Chemical Pty Ltd for providing the metakaolin used in this study. Dr. Rhys Jacob would gratefully like to acknowledge the Alexander von Humboldt Foundation for providing funding to support this work through the Humboldt Research Fellowship. Patrick Keane gratefully acknowledges the Australian Government for funding this research through the Research Training Program. The work of Kriven was funded by the US Army Corps of Engineers through the Engineering Research Development Center and Construction Engineering Research Laboratory in Champaign, IL, USA under Contract Number W9132T-22-C-0011 AJ495.

References

[1] W.M. Kriven, Geopolymers and geopolymer-derived composites, in: M. Pomeroy (Ed.), Encyclopedia of Materials: Technical Ceramics and Glasses, Elsevier, Oxford, 2021, pp. 424–438.
[2] K.J.D. Mackenzie, M. Welter, 22 - geopolymer (aluminosilicate) composites: synthesis, properties and applications, in: I.M. Low (Ed.), Advances in Ceramic Matrix Composites, second ed., Woodhead Publishing, 2014, pp. 545–568.
[3] W.M. Kriven, et al., Corrosion protection assessment of concrete reinforcing bars with a geopolymer coating, Developments in Porous, Biological and Geopolymer Ceramics: Ceram. Eng. Sci. Proc. 28 (9) (2007) 373–381.
[4] T. Bakharev, Durability of geopolymer materials in sodium and magnesium sulfate solutions, Cement Concr. Res. 35 (6) (2005) 1233–1246.
[5] J.L. Provis, J.S.J. Van Deventer, Geopolymers: Structures, Processing, Properties and Industrial Applications, Elsevier, 2009.
[6] A. Palomo, A. Fernández-Jiménez, Alkaline activation, procedure for transforming fly ash into new materials. Part I: applications, in: World of Coal Ash (WOCA) Conference, 2011.
[7] L. Vickers, A. Van Riessen, W.D. Rickard, Fire-resistant Geopolymers: Role of Fibres and Fillers to Enhance Thermal Properties, Springer, 2015.
[8] S. Lee, et al., Impact of activator type on the immobilisation of lead in fly ash-based geopolymer, J. Hazard Mater. 305 (2016) 59–66.
[9] E. Mossini, et al., Pre-impregnation approach to encapsulate radioactive liquid organic waste in geopolymer, J. Nucl. Mater. 585 (2023) 154608.
[10] V.F.F. Barbosa, K.J.D. MacKenzie, C. Thaumaturgo, Synthesis and characterisation of materials based on inorganic polymers of alumina and silica: sodium polysialate polymers, Int. J. Inorg. Mater. 2 (4) (2000) 309–317.
[11] J. Davidovits, The synthesis of alumino-silicate mineral geopolymers, in: J. Davidovits (Ed.), Geopolymer Chemistry & Applications, Institut Geopolymere: Saint-Quentin, 2020.
[12] D.J. Ilham, et al., The potential use of volcanic deposits for geopolymer materials, IOP Conf. Ser. Earth Environ. Sci. 497 (1) (2020) 012035.
[13] J. Deventer, et al., Chemical research and climate change as drivers in the commercial adoption of alkali activated materials, Waste and Biomass Valorization 1 (1) (2010) 145–155.
[14] R. Jacob, et al., Effect of inner coatings on the stability of chloride-based phase change materials encapsulated in geopolymers, Sol. Energy Mater. Sol. Cell. 174 (2018) 271–276.
[15] K. Sankar, A. Sutrisno, W.M. Kriven, Slag-fly ash and slag-metakaolin binders: Part II—properties of precursors and NMR study of poorly ordered phases, J. Am. Ceram. Soc. 102 (6) (2019) 3204–3227.
[16] X. Chen, A. Sutrisno, L.J. Struble, Effects of calcium on setting mechanism of metakaolin-based geopolymer, J. Am. Ceram. Soc. 101 (2) (2018) 957–968.
[17] X. Chen, Setting and nanostructural evolution of metakaolin geopolymer, in: Civil and Environmental Engineering, University of Illinois at Urbana Champaign: Graduate Dissertations and Theses at Illinois, 2017, p. 221.
[18] B. Kenne Diffo, et al., Effect of the rate of calcination of kaolin on the properties of metakaolin-based geopolymers, Journal of Asian Ceramic Societies 3 (1) (2015) 130–138.
[19] S. Samal, I. Blanco, An application review of fiber-reinforced geopolymer composite, Fibers 9 (4) (2021) 23.
[20] S.A. Bernal, et al., Performance of refractory aluminosilicate particle/fiber-reinforced geopolymer composites, Compos. B Eng. 43 (4) (2012) 1919–1928.
[21] G.P. Kutyla, W.M. Kriven, Properties and characterization of alumina platelet reinforced geopolymer composites, J. Am. Ceram. Soc. 103 (9) (2020) 5178–5185.
[22] P.F. Keane, et al., Amorphous self-healed, chopped basalt fiber-reinforced, geopolymer composites, J. Am. Ceram. Soc. 104 (7) (2021) 3443–3451.
[23] A.W. Bhuiya, et al., Bone ash reinforced geopolymer composites, J. Am. Ceram. Soc. 104 (6) (2021) 2767–2779.
[24] G. Lazorenko, A. Kasprzhitskii, Geopolymer additive manufacturing: a review, Addit. Manuf. 55 (2022) 102782.
[25] A.S. Brandvold, A.C.C. Trindade, W.M. Kriven, Rheological assessment of metakaolin-based geopolymer composites through squeeze flow, J. Am. Ceram. Soc. 106 (7) (2023) 4038–4051.
[26] A.S. Brandvold, G.K. Al-Chaar, W.M. Kriven, Isolating the effects of thixotropy in geopolymer pastes, J. Am. Ceram. Soc. 106 (5) (2023) 2797–2807.
[27] G. Franchin, et al., Direct ink writing of geopolymeric inks, J. Eur. Ceram. Soc. 37 (6) (2017) 2481–2489.
[28] M.S. Darmawan, et al., Comparative study of flexural performance of geopolymer and Portland cement concrete beam using finite element analysis, GEOMATE Journal 23 (95) (2022) 1–9.
[29] A.M.M.A. Bakri, et al., Comparison of geopolymer fly ash and ordinary Portland cement to the strength of concrete, Adv. Sci. Lett. 19 (12) (2013) 3592–3595.
[30] Y.-M. Liew, et al., Structure and properties of clay-based geopolymer cements: a review, Prog. Mater. Sci. 83 (2016) 595–629.
[31] N.B. Singh, B. Middendorf, Geopolymers as an alternative to Portland cement: an overview, Construct. Build. Mater. 237 (2020) 117455.
[32] V.O. Shikuku, T. Sylvain, Application of geopolymer composites in wastewater treatment: trends, opportunities, and challenges, in: N. Ramdani (Ed.), Polymer Nanocomposites for Advanced Engineering and Military Applications, IGI Global, Hershey, PA, USA, 2019, pp. 131–149.
[33] L. Ricciotti, et al., Geopolymer materials for bone tissue applications: recent advances and future perspectives, Polymers 15 (5) (2023) 1087.
[34] C. Bagci, et al., Synthesis and characterization of silicon carbide powders converted from metakaolin-based geopolymer, J. Am. Ceram. Soc. 99 (7) (2016) 2521–2530.
[35] P. Keane, et al., Thermal stability of a waste-based alkali-activated material for thermal energy storage, Chemical Thermodynamics and Thermal Analysis 3–4 (2021) 100014.
[36] P.F. Keane, et al., Self-healing glass/metakaolin-based geopolymer composite exposed to molten sodium chloride and potassium chloride, Appl. Sci. 13 (4) (2023) 2615.
[37] A.L. Freire, H.J. José, R.d.F.P.M. Moreira, Potential applications for geopolymers in carbon capture and storage, Int. J. Greenh. Gas Control 118 (2022) 103687.
[38] M. Minelli, et al., Geopolymers as solid adsorbent for CO2 capture, Chem. Eng. Sci. 148 (2016) 267–274.
[39] IRENA, Innovation Outlook: Thermal Energy Storage, International Renewable Energy Agency, Abu Dhabi, 2020.
[40] Y. Yin, et al., Chemical degradation in thermally cycled stainless steel 316 with high-temperature phase change material, Sol. Energy Mater. Sol. Cell. 230 (2021) 111216.
[41] S. Ladkany, W. Culbreth, N. Loyd, Molten salts and applications II: 565 °C molten salt solar energy storage design, corrosion, and insulation, J. Energy Power Eng. 12 (2018).
[42] M. Jonemann, Advanced Thermal Storage System with Novel Molten Salt, Halotechnics, Inc., Golden, Colorado, 2013.
[43] LME Official Prices, in: London Metal Stock Exchange, London Metal Exchange, 2021.
[44] G. Salinas-Solano, et al., High temperature corrosion of inconel 600 in NaCl-KCl molten salts, Adv. Mater. Sci. Eng. 2014 (2014) 696081.
[45] D.J. Duval, S.H. Risbud, J.F. Shackelford, Mullite, in: J.F. Shackelford, R. H. Doremus (Eds.), Ceramic and Glass Materials: Structure, Properties and Processing, Springer US, Boston, MA, 2008, pp. 27–39.
[46] S. Musil, Novel, inorganic composites using porous, alkali-activated, aluminosilicate binders, in: Materials Science and Engineering, University of Illinois at Urbana-Champaign: University of Illinois at Urbana-Champaign Library, 2014.
[47] S.A. Bernal, et al., Mechanical and thermal characterisation of geopolymers based on silicate-activated metakaolin/slag blends, J. Mater. Sci. 46 (16) (2011) 5477–5486.
[48] B. Tempest, et al., Manufacture of full-scale geopolymer cement concrete components: a case study to highlight opportunities and challenges, PCI J. 60 (2015) 39–50.
[49] N. Ranjbar, A. Kashefi, M.R. Maheri, Hot-pressed geopolymer: dual effects of heat and curing time, Cement Concr. Compos. 86 (2018) 1–8.
[50] P. Keane, et al., Microstructural evolution of amorphous self-healing geopolymer composites containing alumina and glass frit, International Journal of Ceramic Engineering & Science 4 (5) (2022) 327–339.
[51] W.M. Kriven, Geopolymer-based composites, Comprehensive Composite Materials II 5 (2018) 269–280.
[52] S.M. Karazi, I.U. Ahad, K.Y. Benyounis, Laser micromachining for transparent materials, in: Reference Module in Materials Science and Materials Engineering, Elsevier, 2017.
[53] C. Piconi, 1.105 - alumina, in: P. Ducheyne (Ed.), Comprehensive Biomaterials, Elsevier, Oxford, 2011, pp. 73–94.
[54] A. Favier, et al., Rheology of Metakaolin Based Geopolymer: Mechanisms and Improvement Potentials, 2012.
[55] A. Ghanbari, et al., Experimental methods in chemical engineering: rheometry, Can. J. Chem. Eng. 98 (7) (2020) 1456–1470.
[56] NETZSCH, Kinexus Series, NETZSCH-geratebau GmbH: Wittelsbacherstrasse 42, 95100 Selb Deutschland, 2023.
[57] T.T. Chen, Introduction to thixotropy analysis using a rotational rheometer [cited 2023; Available from: https://www.tainstruments.com/applications-notes/introduction-to-thixotropy-analysis-using-a-rotational-rheometer/, 2016.
[58] G. Wypych, 3 - typical methods of quality control of plasticizers, in: G. Wypych (Ed.), Handbook of Plasticizers, third ed., ChemTec Publishing, 2017, pp. 85–109.
[59] S.Y. Yong Kim, K.S. Byung, Yong Jae Jun, S.J. Young, S.P. Dong, Multimodal polyolefin resin having high melt strength and shaped product made therefrom, in: U.S.P.a.T. Office (Ed.), DAELIM INDUSTRIAL CO., LTD.: US, 2017.
[60] X. Chateau, 6 - particle packing and the rheology of concrete, in: N. Roussel (Ed.), Understanding the Rheology of Concrete, Woodhead Publishing, 2012, pp. 117–143.
[61] B. Panda, C. Unluer, M.J. Tan, Extrusion and rheology characterization of geopolymer nanocomposites used in 3D printing, Compos. B Eng. 176 (2019) 107290.
[62] F.A. Morrison, Understanding Rheology, Oxford University Press, 2001.
[63] A.S. Brandvold, W.M. Kriven, Influence of temperature on rheological properties during early-stage geopolymerization, J. Am. Ceram. Soc. 107 (2) (2024) 748–759.
[64] C. Lu, et al., Rheology of alkali-activated materials: a review, Cement Concr. Compos. 121 (2021) 104061.
[65] P. Duxson, G.C. Lukey, J.S.J. van Deventer, Physical evolution of Na-geopolymer derived from metakaolin up to 1000 °C, J. Mater. Sci. 42 (9) (2007) 3044–3054.
[66] C. Kuenzel, et al., Ambient temperature drying shrinkage and cracking in metakaolin-based geopolymers, J. Am. Ceram. Soc. 95 (10) (2012) 3270–3277.
[67] A. Pawar, G. Ausias, J. Férec, Dynamics of gas bubbles in fiber suspensions, Int. J. Multiphas. Flow 145 (2021) 103823.
[68] P. Hrma, A.A. Kruger, High-temperature viscosity of many-component glass melts, J. Non-Cryst. Solids 437 (2016) 17–25.